Comparative liquidus equilibria of hypersthene-normative basalts at low pressure

JOHN LONGHI

Lamont-Doherty Geological Observatory, Palisades, New York 19064, U.S.A.

ABSTRACT

The low-pressure liquidus boundaries of natural basaltic liquids have been parameterized as quasi-linear empirical functions of projection coordinates in the Ol-Pl-Wo-Qtz model system. Secondary variables are simple chemical parameters such as Mg′ and the albite and orthoclase fractions of the normative feldspar. These empirical expressions lend themselves to rapid construction of liquidus diagrams as well as forming an integral part of quantitative models of fractional and equilibrium crystallization. The position and reaction relations of the liquidus boundary between olivine (ol) and low-Ca pyroxene (lpyx) are strongly dependent on Mg′ such that olivine reacts with magnesian liquids along the boundary, but precipitates from more ferroan liquids. The transition from a reaction to a crystallization relationship in liquids with intermediate Mg′ is complex, and it is possible for olivine to precipitate during equilibrium crystallization and react during fractional crystallization of the same liquid on the ol-lpyx boundary. A survey of the silicate-liquidus equilibria appropriate to mare, midocean ridge, and calc-alkaline basalts shows that the different alkali contents of these magma types are responsible for the different proportions of mafic and feldspathic components observed in cotectic liquids of each type. Different alkali contents can even produce important differences, such as silica enrichment vs. silica depletion, in the liquid lines of descent (LLD) of parent liquids that have the same initial Mg′ and crystallization sequence. Liquid lines of descent are in general different from the equilibrium crystallization paths that petrologists have employed to construct liquidus diagrams. If one were to use only the plagioclase-component projection, there is the potential for confusing a low-pressure LLD with a high-pressure trend.

INTRODUCTION

Predicting the liquidus equilibria of basaltic magmas has been a goal of petrologists ever since the first melting experiments. Among the first credible attempts to predict liquidus equilibria of natural compositions were those of O'Hara (1968) and Irvine (1970), who employed the bulk compositions and experimentally determined crystallization orders of basalts to construct a series of pseudoternary liquidus diagrams. Walker et al. (1972) carried this graphical approach a step farther by using microprobe analyses of experimentally produced multisaturated liquids to fix the positions of the liquidus boundaries (Fig. 1, top). As recognized by these authors, these diagrams were reliable only for compositions similar to those on which the diagrams were based. Roeder (1975) introduced a second approach that lent itself more readily to calculating fractional crystallization paths. He derived analytical temperature-composition expressions for the olivine and plagioclase liquidus surfaces via multiple linear regression. With these expressions it became possible to compare the calculated liquidus temperatures for olivine and plagioclase of a given basaltic composition: the phase with the highest liquidus temperature was the true liquidus phase as illustrated in the middle panel in Figure 1. Langmuir and Hanson (1981) and Nielsen (1988) mod-

ified this approach considerably by adding additional phases and temperature-composition algorithms for calculating the composition of the solid phases. Ghiorso et al. (1983) developed a regular solution model for basaltic liquids by extracting binary interaction coefficients from a wide range of experimentally produced pairs of crystal + glass (quenched liquid). This model lends itself to the prediction of liquidus equilibria by free energy minimization, as illustrated in the lower panel in Figure 1.

Each approach has its advantages and drawbacks. The major advantage of the graphical approach is its ability to inform the trained observer not only of the immediate liquidus phases of a composition but also of the proportions of important mineral components and of the course of crystallization. To overcome the shortcoming of a limited range of compositions to which these approaches apply, I began a program of parameterizing projected liquidus boundaries more than a decade ago and work is still in progress (Longhi, 1977, 1982, 1987a; Longhi and Pan, 1989). Then, as now, the conceptual framework is the set of quaternary liquidus equilibria in the system CaO-MgO-Al$_2$O$_3$-SiO$_2$ (CMAS) (Presnall et al., 1978; Longhi, 1987b), and the parameterizations account for the shifts in the liquidus boundaries produced by additional natural components such as FeO, TiO$_2$, and alkalies. Over the years these empirical expressions have become more complex

Walker et al. (1972);
this study

Roeder (1975);
Langmuir and Hanson (1981);
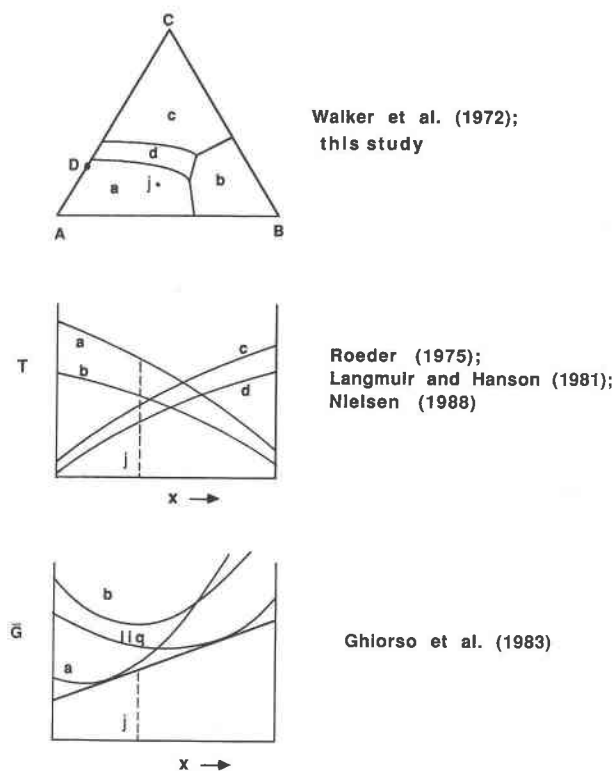Nielsen (1988)

Ghiorso et al. (1983)

Fig. 1. Schematic representation of various methods of predicting liquidus phase equilibria.

as our data have accumulated. Nonetheless, these expressions still lend themselves to rapid construction of liquidus diagrams on personal computers, as well as fast and accurate calculations of fractional crystallization and other processes such as assimilation, magma mixing, and fractional fusion, that are difficult to investigate directly with experiments.

THE MODEL

The basis for the present approach to modeling phase equilibria is the collection of liquidus diagrams for both simple (three or four components) and natural basaltic systems. These diagrams have established not only a general topologic framework of equilibria relating to the basaltic liquidus but also the effects on these equilibria of variable proportions of various mineral components. Thus the important liquidus boundaries that must be modeled are known, as is their general disposition in composition space and the qualitative effects of variation of the major components. For example, several authors (Emslie, 1971; Morse, 1980; Longhi and Pan, 1988a) have employed published data to illustrate that the Fe_2SiO_4 (Fa) and $NaAlSi_3O_8$ (Ab) components shift liquidus boundaries involving plagioclase and a mafic phase in opposite directions when added to the ternary join Mg_2SiO_4-$CaAl_2Si_2O_8$-SiO_2 (Fo-An-Qtz) and that variation of these two components in natural basaltic liquids produces analogous effects.

The present model is actually an amalgam of several submodels: the major submodel deals with silicate equilibria, and there is a slightly different submodel for each oxide phase. The silicate model consists of parameterizations of the compositional dependence of liquidus surfaces in the pseudoquaternary system Ol-Pl-Wo-Qtz (TiO_2, Cr_2O_3, P_2O_5, and K_2O recalculated as orthoclase are projection components). Figure 2 illustrates two three-dimensional views of these surfaces and the various subprojections with which they are more conveniently depicted. Despite the fact that the mineral wollastonite is rarely observed in basaltic rocks, I employ the wollastonite (Wo = $CaSiO_3$) component, rather than the conventional diopside component, as the calcium silicate component for two reasons. First, the Wo component expands the compositional limits of the system so as to include compositions transitional between tholeiites and alkali basalts; and second, the Wo component causes less parallax distortion of projections of the ol-plag, ol-lpyx, and lpyx-plag surfaces onto the Ol-Pl-Qtz plane than does the diopside projection (Longhi, 1987b, Fig. 10), which is a distinct advantage in portraying the liquidus equilibria of magmas in which augite crystallizes after olivine, plagioclase, or low-Ca pyroxene. The reader should keep in mind, however, that the mineral wollastonite is never a saturating phase and the projection is optical rather than thermodynamic. Appendix 1 contains a brief discussion of the components for the other submodels.

The silicate model contains quasi-linear expressions for the location of the following liquidus boundaries within the Ol-Pl-Wo-Qtz system: ol-sp (aluminous), ol-plag, ol-lpyx, lpyx-plag, sil-lpyx, ol-aug, lpyx-aug, and opx-pig. No attempt has been made to separate protoenstatite from the other low-Ca pyroxenes because experimental data on natural compositions is limited and because protoenstatite is restricted to extremely magnesian liquids (Longhi and Pan, 1988a) and is rare. All of the phase boundaries except those that involve augite are represented by temperature-independent expressions with the form of simple planes

$$Ol\{Wo\} = a(Fe', NAB, NOR)\cdot Qtz\{Wo\} + b(Fe')\cdot Wo + c(Fe', NAB, NOR)$$

or

$$Qtz\{Wo\} = a(Fe', NAB, NOR)\cdot Ol\{Wo\} + b(Fe')\cdot Wo + c(Fe', NAB, NOR)$$

or

$$Wo = a(Fe', NAB, NOR)\cdot Ol\{Wo\} + b(Fe', NAB, NOR)\cdot Qtz\{Wo\} + c(Fe', NAB, NOR)$$

where convenience of manipulation dictates the choice of dependent and independent variables. The projection coordinates are in mole units, in order to facilitate conversion to other sets of components or to other units. Wo is the quaternary coordinate of the wollastonite component in Figure 2; Ol{Wo} and Qtz{Wo} are ternary coordinates in the {Wo} subprojection (Fig. 2); NAB and NOR
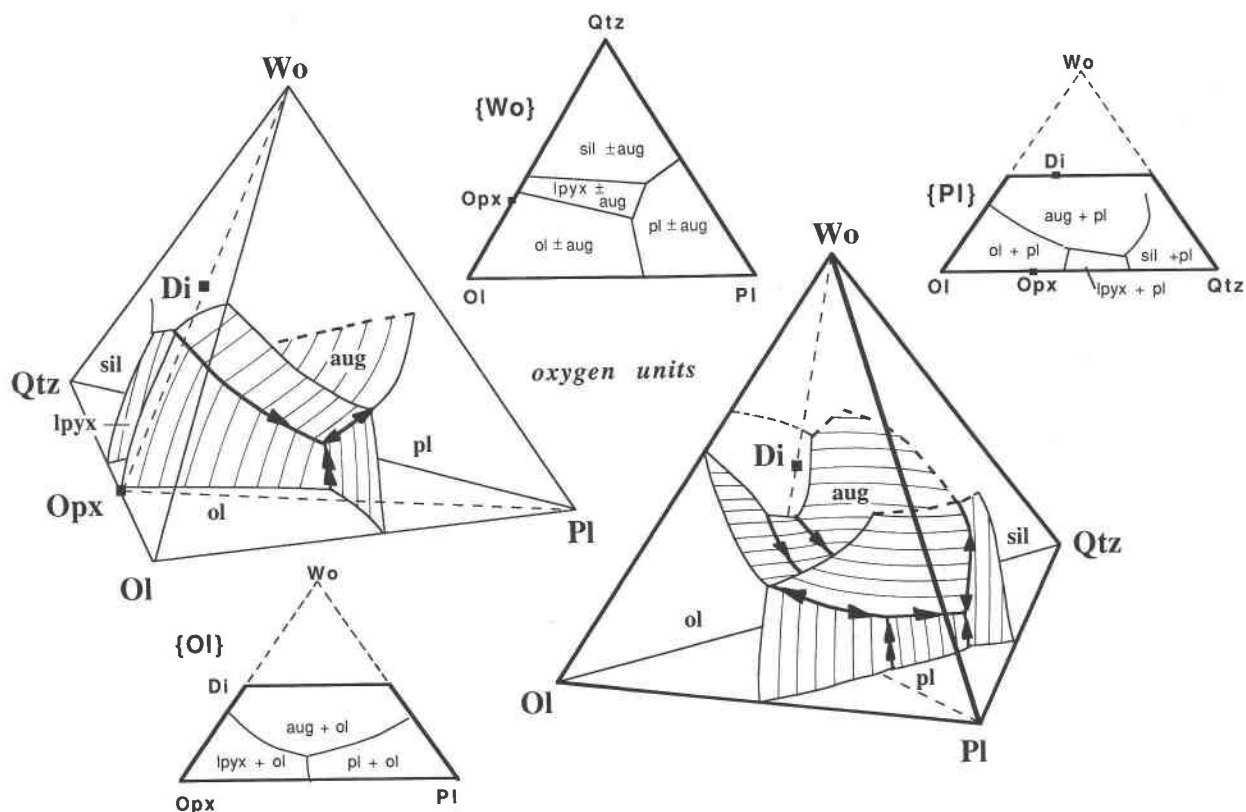
Fig. 2. Pseudoquaternary liquidus surface and subprojections for silicate liquidus equilibria in terms of O units in the model system Ol-Pl-Wo-Qtz. In the three-dimensional diagrams heavy curves represent pseudoquaternary equilibria (liquid plus three solid phases; light curves represent pseudoternary equilibria (liquid plus two solid phases); dashed curves involve the mineral wollastonite; solid curves do not. Arrows show direction of decreasing temperature; single arrows are cotectics; double arrows are reaction curves. Abbreviations of phase names: ol = olivine; pl = plagioclase; lpyx = low-Ca pyroxene (either opx = orthopyroxene or pig = pigeonite); aug = augite; sil = silica phase (either tridymite or cristobalite).

are the mole fractions of albite and orthoclase in the normative feldspar, respectively; Fe' is FeO/(FeO + MgO) or $1 - Mg'$ in mole units; and a, b, and c are empirical functions of slope and intercept. Equations for these various parameters are listed in Appendix 1. The ol-aug, lpyx-aug, and opx-pig phase boundaries are represented by expressions of the form

$$Wo = d(Fe', NAB, NOR) \cdot Ol\{Wo\}$$
$$+ e(Fe', NAB, NOR) \cdot Qtz\{Wo\}$$
$$+ f(Fe', NAB, NOR) + k(1 - Pl\{Wo\})^n$$

where d, e, and f are empirical functions and k and n are empirical constants. Because the exponential term is important only for low values of Pl{Wo}, these expressions are planar for most of the range of basaltic composition. Other relevant phase boundaries, such as ol-sil, sil-plag, and plag-sp are approximated by extrapolation.

With these expressions it is a straightforward process to test a basaltic composition for its liquidus phase or to construct a phase diagram. The simplest type of diagram to generate is the version of the {Wo} projection illustrated in Figure 2 in which the Fe', NAB, NOR, and Wo parameters are held constant at some low Wo value at which augite is not stable. In this case the diagram is an edge-on section through the series of three-dimensional surfaces beneath the augite saturation surface and the field boundaries involve only two solid phases, e.g., ol and plag. Face-on projections of the three-dimensional liquidus saturation surfaces, such as the {Ol} and {Pl} diagrams illustrated in Figure 2, produce field boundaries involving three solid phases, e.g., ol, plag, and lpyx. Generating these diagrams requires solving the expressions for two adjacent surfaces (in this case, ol-plag and ol-lpyx) simultaneously, while holding Fe', NAB, and NOR constant. If the expressions for the adjacent surfaces do not contain an exponential term, then it is a straightforward matter to solve the two expressions analytically and eliminate one of the major variables. When one of the two expressions contains an exponential term, then a numerical solution can be obtained quickly because the exponential term is small over most of the range of composition.

The expressions for phase boundaries listed in Appendix 1 have been tested against a representative data base
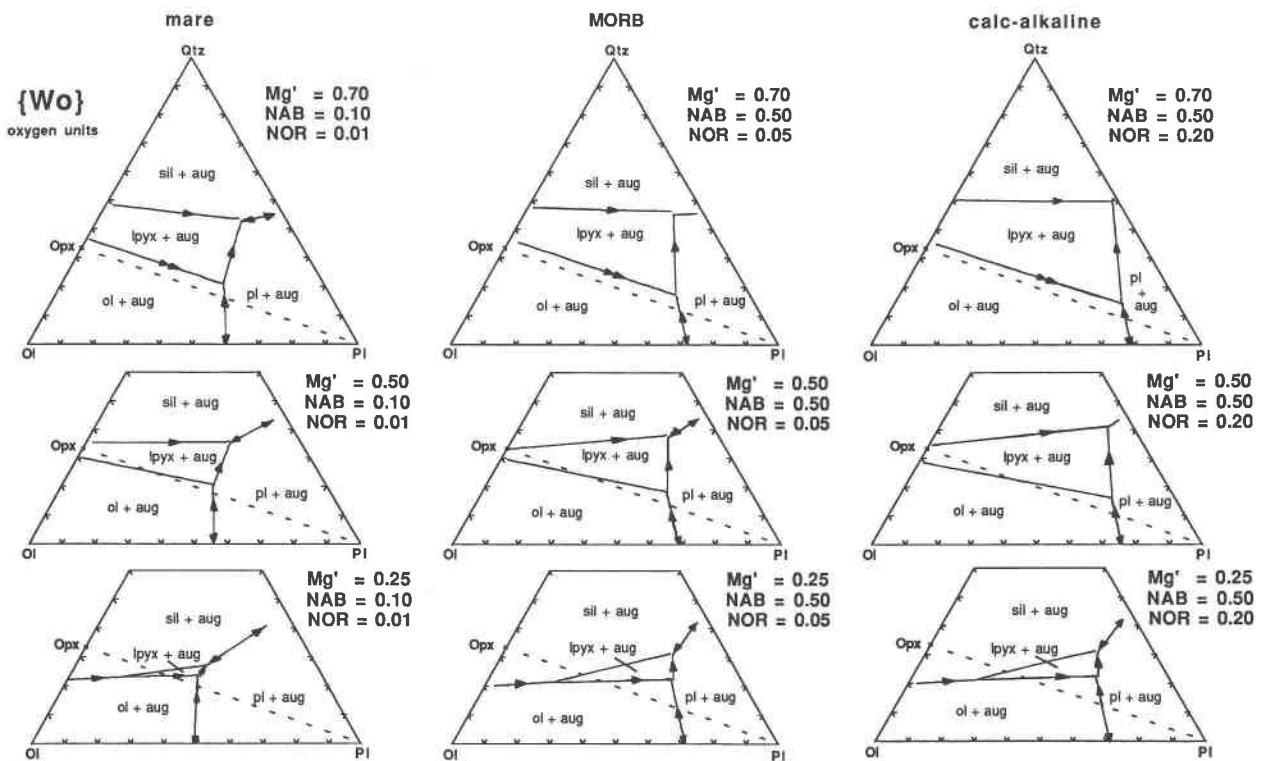
Fig. 3. Systematic variation of the topology of the augite liquidus surface with composition. Columns have alkali contents representative of mare (NAB = 0.1, NOR = 0.01), MORB (NAB = 0.5, NOR = 0.05), and calc-alkaline (NAB = 0.5, NOR = 0.2) magmas. Rows have Mg' representative of primitive (0.7), intermediate (0.5), and evolved (0.25) basalts. Arrows point in direction of decreasing temperature; double arrows indicate reaction relation exclusive of augite. Projection equations in O units are $Ol\{Wo\} = 2(FeO + MgO + MnO + 2Fe_2O_3)/\Sigma$, $Qtz\{Wo\} = [2SiO_2 - FeO + MgO + MnO + 2Fe_2O_3 - 2Al_2O_3 - 2CaO - 10(K_2O + Na_2O)]/\Sigma$, and $Pl\{Wo\} = 8(Al_2O_3 + Na_2O - K_2O)/\Sigma$, where Σ is the sum of the numerators of the three equations and chemical symbols refer to mole concentration units.

from the literature. The data include hypersthene-normative lunar, meteoritic (eucrite, shergottite, nakhlite), and terrestrial (MORB, calc-alkaline) compositions. The ranges of the composition variables are Fe' = 0.26–0.98, NAB = 0.09–0.56, and NOR = 0.01–0.43, although the practical range of the model is somewhat less than the full random range of these variables as discussed below. The figures in Appendix 1 illustrate the ability of the expressions to predict the composition of their respective liquidus boundaries independent of temperature. When the expressions of the temperature-independent phase boundary are coupled with various empirical temperature-composition expressions for mineral-liquid pairs (e.g., Roeder and Emslie, 1970; Drake, 1976; Longhi et al., 1978), it is possible to calculate the liquidus temperature and the temperatures of subsequent phase appearances and disappearances (resorption). Longhi (1987a) and Longhi and Pan (1988b) have illustrated the ability of the combined model to reproduce experimentally determined crystallization-resorption sequences for mare and eucritic basalts, respectively. No attempt has been made to evaluate the expressions for ol-sp and sil-lpyx because of a lack of a wide data base.

COMPARATIVE LIQUIDUS EQUILIBRIA

Perhaps the most important function of liquidus diagrams is to give petrologists a sense of why magmas crystallize the way they do. The graphic capabilities of the model make it possible to study not only the phase equilibria characteristic of individual magmatic compositions but also to compare the phase equilibria of different families of magmas. Figures 3, 4, and 5 provide such a comparison in terms of the augite, olivine, and plagioclase liquidus surfaces, respectively. In each figure the columns differ according to normative feldspar composition in the manner of some representative mare, midocean ridge, and calc-alkaline basalts; whereas the rows differ according to Mg' (or 1 − Fe'). One of the limitations of the model for liquidus boundaries is that there is not a parallel set of parameterizations for solid compositions, which are necessary to predict directions of falling temperature, reaction relations, and extrema of temperature along phase boundaries. Various empirical temperature-composition expressions do permit the calculation of mineral compositions from a single liquid composition (e.g., Drake, 1976; Nielsen and Dungan, 1983), so there is no obstacle
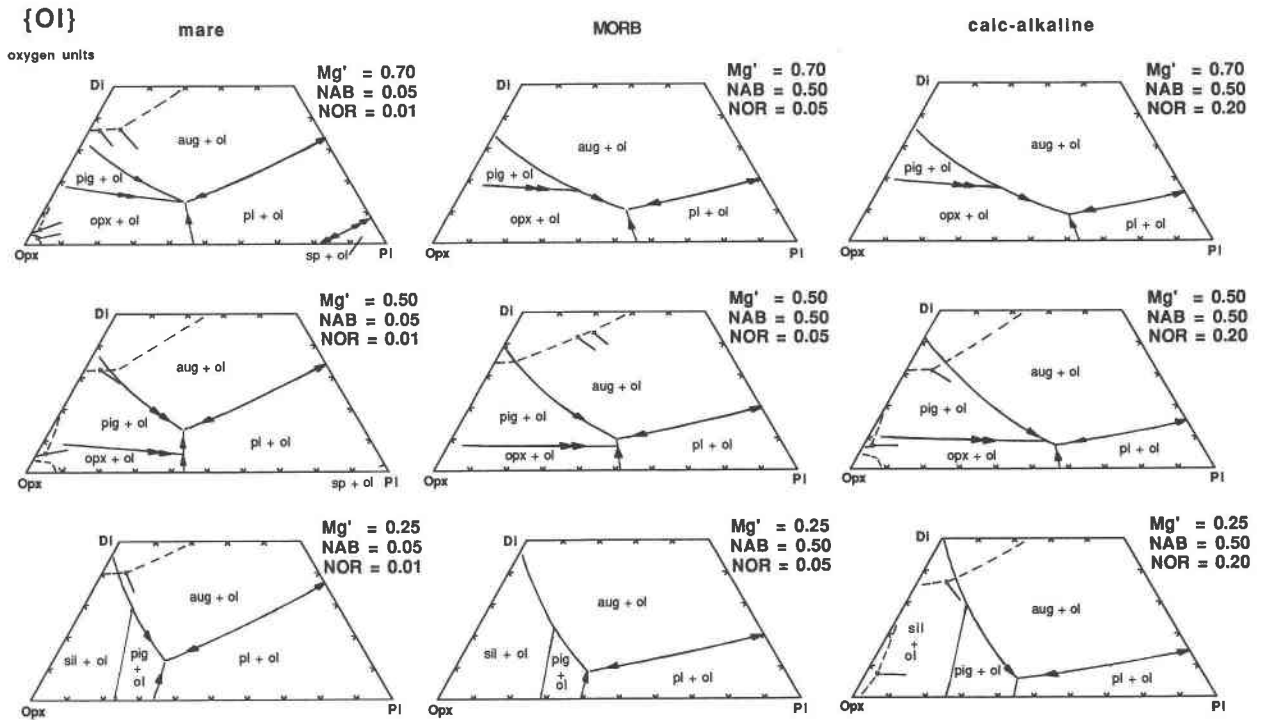
Fig. 4. Systematic variation of the topology of the olivine liquidus surface with composition. Columns have alkali contents representative of mare (NAB = 0.1, NOR = 0.01), MORB (NAB = 0.5, NOR = 0.05), and calc-alkaline (NAB = 0.5, NOR = 0.2) magmas. Rows have Mg' representative of primitive (0.7), intermediate (0.5), and evolved (0.25) basalts. Dashed lines enclose areas of solid solution. Arrows point in direction of decreasing temperature; double arrows indicate reaction relation exclusive of olivine. Projection equations in terms of O units are Opx{Ol} = 3[2SiO$_2$ − FeO + MgO + MnO + 2Fe$_2$O$_3$ − 2CaO − 2Al$_2$O$_3$ − 10(K$_2$O + Na$_2$O)]/Σ, Wo{Ol} = 3(CaO − Al$_2$O$_3$ + K$_2$O + Na$_2$O)/Σ, and Pl{Ol} = (8Al$_2$O$_3$ + 8Na$_2$O − 8K$_2$O)/Σ where Σ is the sum of the numerators of the three equations and chemical symbols refer to mole concentration units.

to quantitative modeling of crystallization. However, the problem remains for rapid graphical representation. In most situations this is not a serious problem because the mineral compositions appear fixed or of limited extent in projection, but difficulties can arise with the interpretation of liquidus boundaries involving augite, whose composition varies considerably (e.g., Longhi, 1987b). To allow for these uncertainties the following convention has been adopted in the phase diagrams: where the compositions of the solid phases are well constrained by experimental data, arrows are drawn indicating the direction of falling temperature, with single arrows indicating cotectic curves and double arrows indicating reaction curves; where the solid compositions are not well constrained, no arrows are drawn; also, the representation of reaction relations is made without regard to the relation of the projection phase, so, for example, in the case of the lpyx-plag-ol curve along which olivine reacts with liquid, the curve appears even (single arrow) in the {Ol} projection and odd (double arrow) in the {Pl} projection.

Figure 3 illustrates some general features in liquids saturated with augite. However, because the projection from the Wo component provides a nearly edge-on view of the various surfaces (ol-pl, ol-lpyx, lpyx-pl, sil-lpyx) that lie

beneath the augite surface (Longhi and Pan, 1988a), the diagrams also depict the approximate positions of various augite-undersaturated liquidus boundaries. In other words, the ol-pl boundary plots in approximately the same position as the ol-pl-aug boundary over a considerable range of Wo content. The same is not true for projections from the Di component. The most important features are the shift of the ol-pl and lpyx-pl liquidus boundaries toward the Ol-Qtz join as Mg' decreases and toward the Pl-Qtz join as alkalies increase, the gradual contraction of the lpyx field as Mg' decreases, and the overall differences in the normative plagioclase content of multisaturated liquids among the three families of magmas. Numerous authors, starting with Bowen (1915), have demonstrated one or more of these effects based upon analogies with simpler systems, so Figure 3 is merely a clearer, more quantitative depiction of what is already known. Nonetheless, some of the implications are worth mentioning. For example, the ratio of plagioclase to mafic mineral components is greatest for calc-alkaline cotectic liquids and least for mare cotectic liquids. Thus cotectic calc-alkaline volcanics should have the highest ratios of plagioclase/mafic in their phenocryst assemblages, cumulates formed from cotectic calc-alkaline magmas (troctolite,
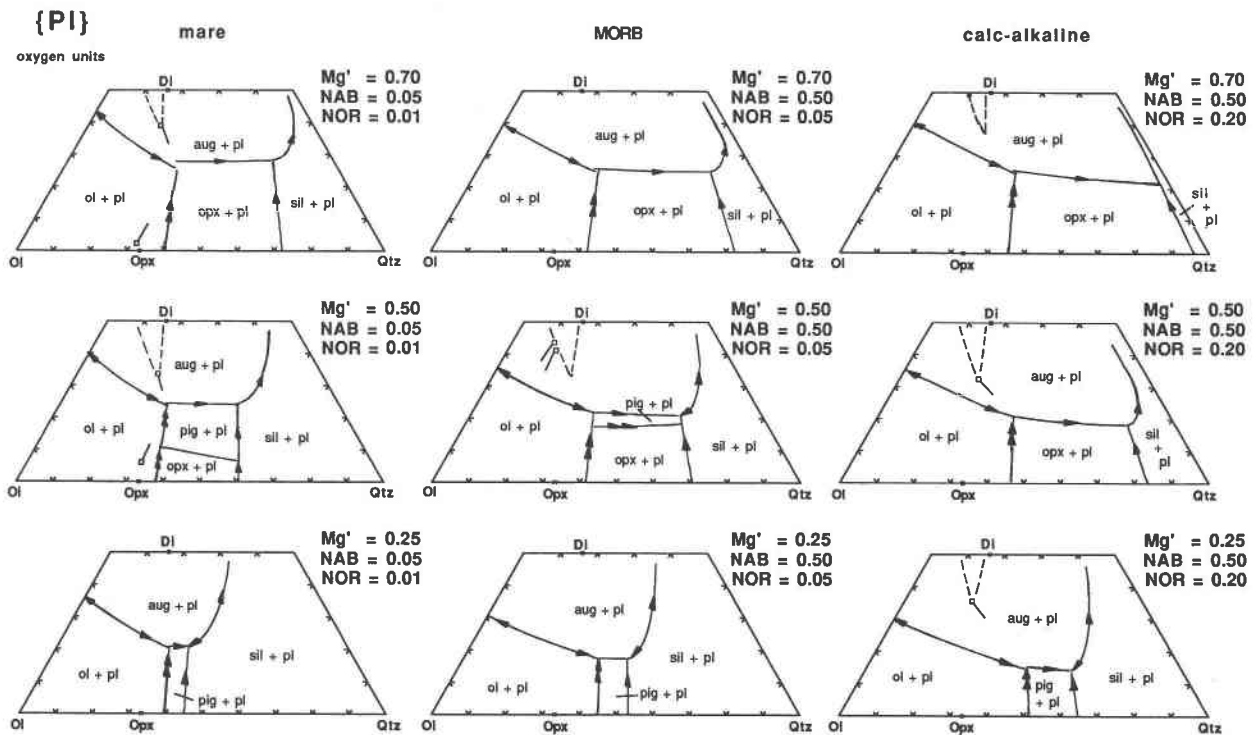
Fig. 5. Systematic variation of the topology of the plagioclase liquidus surface with composition. Columns have alkali contents representative of mare (NAB = 0.1, NOR = 0.01), MORB (NAB = 0.5, NOR = 0.05), and calc-alkaline (NAB = 0.5, NOR = 0.2) magmas. Rows have Mg' representative of primitive (0.7), intermediate (0.5), and evolved (0.25) basalts. Dashed lines enclose areas of solid solution. Arrows point in direction of decreasing temperature; double arrows indicate reaction relation exclusive of plagioclase. Projection equations in terms of O units are Ol{Pl} = $2(FeO + MgO + MnO + 2Fe_2O_3)/\Sigma$, Wo{Pl} = $3(CaO - Al_2O_3 + K_2O + Na_2O)/\Sigma$, and Qtz{Pl} = $[2SiO_2 - FeO + MgO + MnO + 2Fe_2O_3) - 2Al_2O_3 - 2CaO - 10(K_2O + Na_2O)]\Sigma$ where Σ is the sum of the numerators of the three equations and chemical symbols refer to mole concentration units.

gabbro, norite) should also have the highest ratios of plagioclase/mafic, and in general calc-alkaline rocks should be the most leucocratic. Exceptions to these rules are commonplace and indicate the intervention of some additional process such as crystal accumulation.

The most complex aspects of phase equilibria in Figure 3 are associated with the contraction and eventual disappearance of the lpyx (± aug) field as Mg' decreases. As Mg' decreases, the sil-lpyx boundary rotates and moves away from Qtz more rapidly than ol-lpyx. At Mg' ~ 0.4 the sil-lpyx curve overtakes the ol-lpyx curve first along the Ol-Qtz join and then, as Mg' continues to decrease, farther into the interior of the diagram, pinching out the lpyx (± aug) field and generating the ol-sil boundary. Eventually the lpyx (± aug) field disappears completely when the point ol + sil + lpyx + aug reaches the lpyx + plag + sil + aug eutectic. The liquidus boundary expressions duly reproduce this phenomenon; however, this mechanism for the reappearance of olivine at the expense of low-Ca pyroxene (pigeonite in low Mg' liquids) may be significant only in mare basalts and in calc-alkaline volcanics where silica minerals crystallize well before Fe-rich olivine. Reduction of magnetite or reaction of ul-

vöspinel with liquid may stabilize Fe-rich olivine at the expense of low-Ca pyroxene in the absence of a silica phase in residual terrestrial magmas (Frost et al., 1988); and the emergence of an expanding two-liquid field (Hess et al., 1975, 1978; Longhi, 1990) may obscure this reaction in residual KREEP magmas.

The rotation and translation of the ol-lpyx boundary away from Qtz also has important implications for reaction relations among olivine, low-Ca pyroxene, and liquid. First, the rotation of the ol-lpyx curve keeps the point involving ol + lpyx + plag (± aug) on the high-silica side of the Opx-Pl join. This location ensures a reaction relation between olivine and liquids saturated with low-Ca pyroxene and plagioclase (± aug) over a very wide range of compositions. [Actually, the reference line is the tie line joining coexisting low-Ca pyroxene and plagioclase. This tie line is rotated slightly counterclockwise relative to the Opx-Pl join because of solid solution of (Mg, Fe, Ca)Al$_2$SiO$_6$ components in pyroxene and Ca(Mg,Fe)Si$_3$O$_8$ components in plagioclase, but because the rotation is small and the pivot point is near the middle of the Opx-Pl join, the difference between the two lines is not significant near the peritectic.] Second, as Mg' decreases, the

ol-lpyx boundary will change from odd to even. Unfortunately, the change cannot be read reliably from these diagrams by drawing a tangent from a point on the ol-lpyx boundary to the Ol-Opx join for a variety of reasons: (1) the tangent to a given point on the ol-lpyx boundary must also be tangent to the liquid path, but the boundaries generated in these projections have constant Mg′ (Fig. 4); (2) it is the intersection of the tangent with the ol-lpyx tie line that is relevant and this tie line is difficult to locate precisely because of solid solution of Tschermak's (aluminous) components in lpyx; (3) the true boundaries are curved slightly.

There are additional complications associated with the Mg′ dependence of the ol-lpyx boundary. First, where the boundary is even with respect to fractional crystallization, the liquid path along the ol-lpyx boundary will be more steeply inclined away from the Qtz{Wo} vertex than the equilibrium crystallization path beginning at the same point, because Mg′ decreases more rapidly per unit of crystallization in a liquid undergoing fractional crystallization than in the same liquid undergoing equilibrium crystallization (cf. Fig. 5, Longhi and Pan, 1988b). Also, Bowen and Schairer (1935) demonstrated that for fractional crystallization conditions the ol-lpyx boundary in the MgO-FeO-SiO$_2$ system changes from odd to even as Mg′ decreases at a unique neutral point at intermediate Mg′; however, there is no unique neutral point for equilibrium crystallization conditions: the change from odd to even is a function of bulk composition. More importantly, the transition from odd to even for equilibrium crystallization occurs at higher Mg′. This means that it is possible for a liquid crystallizing olivine to reach the ol-lpyx boundary and begin to cocrystallize low-Ca pyroxene and a small amount of olivine and, subsequently, to crystallize only low-Ca pyroxene if the olivine is abruptly removed or to resorb the olivine if the crystallization rate increases. Perhaps the clearest illustration of the change from odd to even in ternary systems is contained in Figures 15.21 and 15.22 in Morse (1980). Because of the additional components in the natural system, the neutral point becomes a volume in hyperspace whose compositional range is difficult to predict.

A possible manifestation of the different transitions from even to odd in equilibrium and fractional crystallization along the ol-lpyx boundary is in the abrupt contact between harzburgites with cumulus-appearing olivine and overlying bronzitites with no olivine in the cyclical portion of the ultramafic zone of the Stillwater Complex (Jackson, 1961; Raedeke and McCallum, 1984). Irvine (1970) suggested that magma fractionating along a strongly curved ol-lpyx boundary (convex toward Qtz) initially cocrystallized ol and lpyx and then, as the tangent to the curved liquid path swept across the opx end of the ol-opx tie line, moved off the ol-lpyx boundary and crystallized only opx. However, there is no experimental evidence of the strong curvature of the ol-opx boundary in natural compositions that would be necessary to change the proportions of cocrystallizing ol and opx from ∼50/50 to

0/100 in less than 100 m of section; rather, experiments show that the ol-lpyx boundary is relatively straight in intermediate to moderately magnesian liquids (Longhi and Pan, 1988a). Furthermore, if a magma saturated with olivine and orthopyroxene were simply crystallizing along an even portion of the ol-lpyx boundary and then crossed to an odd portion, some widespread evidence of reaction would be expected. However, if the magma were situated on a region of the ol-lpyx boundary that was even with respect to equilibrium crystallization and odd with respect to fractional crystallization, and if turbidity currents as suggested by Irvine (1980) and Raedeke and McCallum (1984) deposited suspensions of olivine on the floor of the magma chamber, then the olivine would continue to grow (slightly) wherever it was present, but once all the olivine settled out of a given level, no more would crystallize. The result would be similar to what is observed: layers with cumulus olivine lacking evidence of the reaction to form orthopyroxene overlain by olivine-free layers.

Figure 4 illustrates changes in liquidus boundaries over the same range of composition as Figure 3 but from a different perspective, a projection from the olivine component. Representative pyroxene compositions with partial tie lines to liquids along the boundary curves are shown where experimental data exist. The various phase boundaries have the same curvature as their analogues in the CMAS system (e.g., Longhi, 1987b) with the exception of the aug-pig-ol boundary which is apparently convex toward Wo in the natural system and slightly convex toward Opx in CMAS. The reason for this discrepancy is not apparent, but Irvine (1970) also inferred a curvature for the augite-lpyx-ol boundary similar to that shown here from a different data set. Orthopyroxene-pigeonite relationships are the most important features of Figure 4. The opx-pig-ol boundary moves to lower Wo as Mg′ decreases but is hardly affected by changing alkalies. However, increasing alkalies shift the lpyx-plag-ol boundary to higher Pl contents, which in turn permits the lpyx-aug-ol and opx-pig-ol curves to extend to higher Pl contents. As a result, orthopyroxene remains the stable low-Ca pyroxene in the peritectic assemblage ol + lpyx + aug + plag to lower values of Mg′ in calc-alkaline liquids than in MORB or mare basalts. Thus the shift in the lpyx-plag-ol surface provides a rational explanation for the seemingly contradictory observation that the higher temperature polymorph, orthopyroxene, is stable to lower Mg′ and temperature than pigeonite in equivalently saturated magmas (e.g., Baker and Eggler, 1987). Also of interest are the rapid contraction of the sp + ol field with decreasing Mg′ and increasing alkalies and the encroachment of the pig + ol field by the sil + ol field. When Mg′ decreases below 0.12, the pi + ol field disappears completely in marelike liquids (Longhi and Pan, 1988a). However, analogous to the effect of stabilizing orthopyroxene with respect to pigeonite, increasing alkalies also appear to stabilize pigeonite to lower Mg′ with respect to olivine and silica by shifting the lpyx-plag-ol boundary away from the advancing lpyx-sil-ol boundary.

TABLE 1. Compositions of model parent magmas

	Mare	MORB	Calc-alk	MORB'
SiO_2	46.9	53.1	54.9	51.2
TiO_2	1.63	1.97	0.59	2.05
Al_2O_3	8.5	15.1	15.9	15.7
Cr_2O_3	0.02	0.01	0.01	0.01
FeO	12.6	8.97	8.31	9.35
MgO	10.1	7.58	6.38	7.90
MnO	0.11	0.13	0.13	0.14
CaO	13.6	9.91	9.57	10.3
K_2O	0.02	0.21	1.37	0.22
Na_2O	0.27	2.97	2.86	3.1
Mg'	0.59	0.60	0.58	0.60
NAB	0.06	0.48	0.43	0.48
NOR	0.003	0.02	0.13	0.02

Figure 5 illustrates liquidus boundaries on the plagioclase saturation surface over the same range of compositions as Figures 3 and 4. Representative pyroxene compositions with partial tie lines to liquids along the boundary curves are shown where experimental data exist. Perhaps the most striking feature is the large variation in the apparent extent of the lpyx + pl fields. Some of this variation is the result of the contraction of the lpyx field with decreasing Mg'; however, much of the expansion of the lpyx + pl field as alkalies increase at constant Mg' is a distortion of composition space caused by the low-angle approach of the lpyx-pl (± aug) boundary to the Pl-Qtz join as illustrated in Figure 3. Figure 5 also depicts the succession of orthopyroxene by pigeonite as Mg' decreases, but not as clearly as Figure 4. At Mg' = 0.7 orthopyroxene is the only low-Ca pyroxene on the plagioclase saturation surface, and at Mg' = 0.25 pigeonite is the only low-Ca pyroxene. At Mg' 0.5 only the mare and MORB panels show orthopyroxene and pigeonite together on the plagioclase saturation surface. Given the set of NAB and NOR parameters chosen for the calc-alkaline liquids, pigeonite does not appear until Mg' ~ 0.45.

LINES OF DESCENT

Being able to predict liquidus equilibria for a wide range of compositions makes it possible to compare lines of descent of classes of magmas in addition to illustrating differences in phase equilibria. There are myriad possible crystallization paths to compare, but to simplify matters I have chosen to discuss the fractionation of one parent liquid composition from each of the three groups (mare, MORB, calc-alkaline). Furthermore, I have modified the compositions (Table 1), by trial and error, such that they will all have a similar initial Mg', crystallization order (ol + pl → ol + pl + aug → pl + aug + lpyx → pl + aug + lpyx + sil), and low Qtz{Wo} coordinate. Because these constraints match MORB compositions most closely, neither the mare nor calc-alkaline compositions provide typical examples of crystallization of their respective magma types. I obtained a fourth composition, MORB', by reducing the SiO_2 concentration in the model MORB magma to illustrate the effects of initial silica content. These compositions were used in the calculations carried out with the fractional crystallization program described in

detail by Longhi and Pan (1989), which is described briefly in Appendix 1.

It would be a straightforward matter to illustrate the array of liquidus boundaries encountered by each fractionating liquid at each step of the way in terms of the {Wo}, {Ol}, and {Pl} projections. In the interest of conserving space, however, I have chosen to illustrate only the array of liquidus boundaries encountered by the model calc-alkaline composition at the appearance of each new phase in terms of the {Pl} projection (Fig. 6). Figure 6 differs from Figure 5 in that all three liquid variables (Mg', NAB, NOR) are changing simultaneously in response to crystallization. Analogous diagrams for the mare and MORB compositions are qualitatively similar. The dashed curve is the LLD. One point of interest is that although the liquid (Mg' = 0.51) at the first appearance of augite appears to be very close to saturation with pigeonite (Fig. 6b), increasing NOR manages to keep shifting the ol-lpyx boundary toward Qtz away from the advancing liquid, thus allowing a long interval of crystallization of ol + pl + aug, as evidenced by the relatively low value Mg' (0.18) in the residual liquid when pigeonite finally does appear (Fig. 6c). Figure 7 illustrates the aggregate mare, MORB, and calc-alkaline liquid lines of descent (LLD) in terms of the {Wo} projection (Fig. 7a) and the AFM diagram (Fig. 7b). In Figure 7a the liquidus boundaries appropriate to the parental MORB composition provide a frame of reference; the symbols mark liquid compositions at the appearance of new phases (p = pl; a = aug; 1 = lpyx; i = ilm; s = sil); the filled circle is the lower silica MORB' composition, which will be discussed separately. The sequence of phases is the same for the MORB and calc-alkaline compositions, but in the mare sequence silica and ilmenite reverse their orders. There is no special significance in this reversal of phase appearance. It is merely a result of arbitrary choices of initial TiO_2 concentrations. Thus in each case the LLD extends only to the point where both silica and ilmenite are present; if the calculations were to be continued, the three LLD would ultimately converge. As suggested by Figure 3, the three lines of descent in Figure 7a are offset from one another because of the different alkali contents. The mare LLD is inclined strongly toward the Ol-Qtz join, an indication that the effects of decreasing Mg' overwhelm those of increasing alkalies in low-alkali compositions. The mare LLD actually moves away from Qtz{Wo} after reaching silica saturation in response to a shift in liquidus boundaries produced when TiO_2 concentration increases above 4 mol% (Longhi, 1987a). The MORB LLD follows fairly closely the liquidus boundaries appropriate for the parental liquid, a sign that the effects produced by decreasing Mg' and increasing alkalies tend to balance one another. However, even though the calc-alkaline parent magma composition appears very similar to that of the MORB parent, its LLD is inclined slightly to the Pl-Qtz join, a sign that the effect of alkalis is slightly stronger than the effect of Mg'. In this case it is the geometric increase in the nonnegligible K_2O concentration that has the greatest effect.
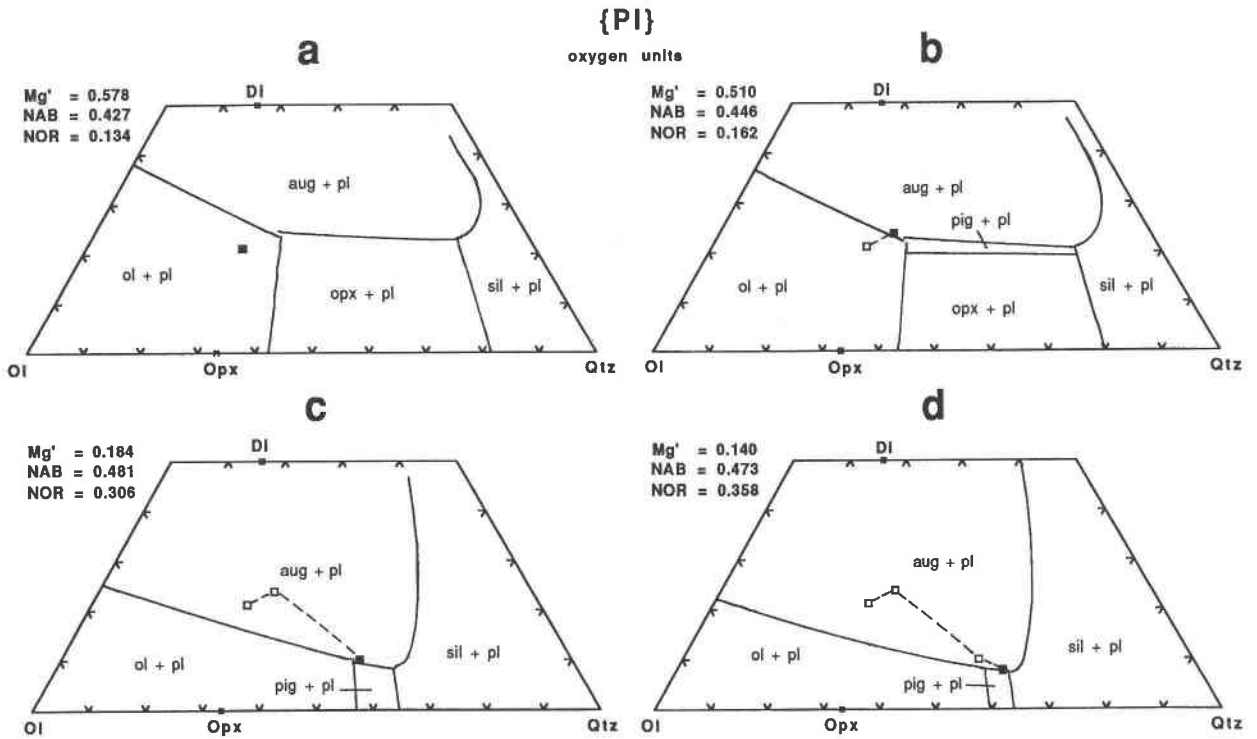
Fig. 6. Array of liquidus boundaries projected from plagioclase encountered when a new phase appears during fractional crystallization of the model calc-alkaline composition (Table 1). (a) Initial cosaturation of ol and pl. (b) First appearance of aug. (c) First appearance of pig, ol ceases crystallization. (d) First appearance of sil. Filled squares are current liquid compositions. Compositional parameters (Mg', NAB, NOR) apply to the current liquid. Dashed curve is the liquid line of descent (LLD).

In response to the shift of the sil-lpyx boundary away from Qtz{Wo} as Mg' decreases rapidly during fractional crystallization, all three residual liquids reach silica saturation at much lower values of the Qtz{Wo} coordinate than would have been predicted from the parameters of their parent compositions.

For the sake of clarity, the LLD of the MORB' composition is not shown. Initially the MORB' LLD follows
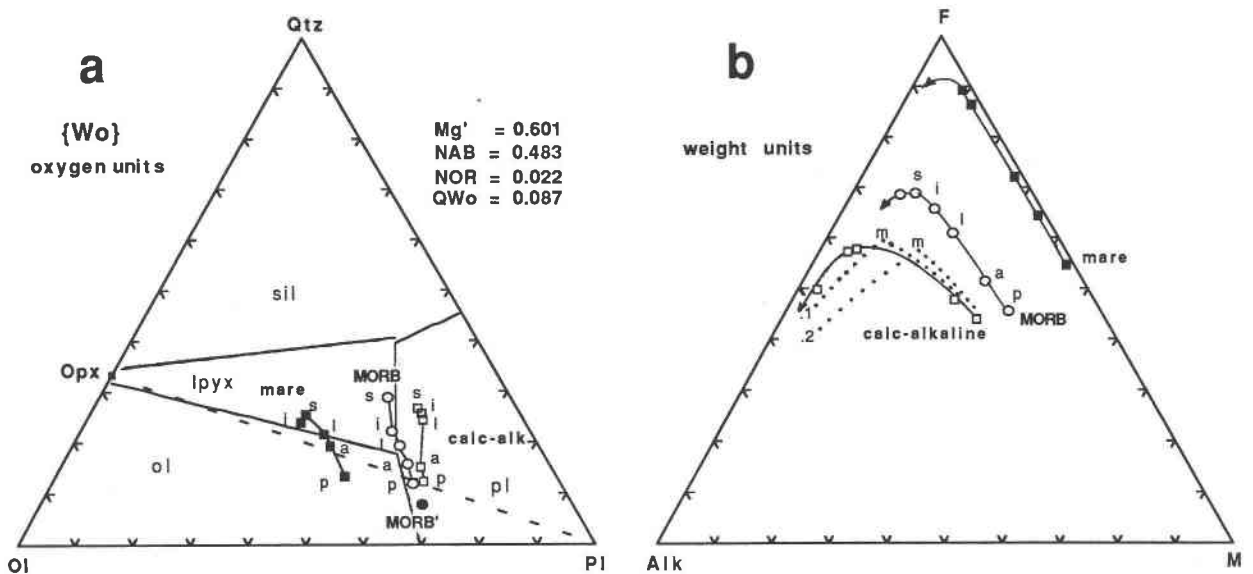
Fig. 7. Comparison of liquid lines of descent in {Wo} (a) and AFM (b) projections. Letters refer to new phases as explained in the text. Alk = K_2O + Na_2O; M = MgO; F = FeO + Fe_2O_3 in weight units.

in the same direction as the MORB LLD in Figure 7a, but it does not reach the approximate position of the MORB bulk composition until it is more than 60% crystallized (ol + pl + aug), at which point ilmenite begins to crystallize and the LLD moves mores off the MORB LLD to the right and eventually crosses the calc-alkaline LLD. Ferroan pigeonite eventually appears at 89% crystallization vs. 58% for pigeonite in the MORB LLD. The reversal of the orders of appearance of ilmenite and pigeonite as well as the much later appearance of pigeonite are caused by the MORB′ composition lying closer to the ol-pl-aug thermal divide than does the MORB composition. The MORB′ composition not only has farther to go to reach the lpyx saturation surface, but it also makes less progress per unit of crystallization in the {Wo} projection because there is less compositional separation between the crystals and the liquid.

The mare, MORB, and calc-alkaline LLDs are also clearly separable in the AFM diagram (Fig. 7b), which petrologists commonly employ to distinguish trends of tholeiitic and calk-alkaline lavas. Tholeiitic trends are marked by increasing F/M with only modest increases in the Alk coordinate until high values of F/M; calc-alkaline trends are marked by rapidly increasing Alk coordinate at intermediate values of F/M. In Figure 7b it is obvious that the different alkali contents of the parent liquids are responsible not only for the different starting points, but also the different trajectories. All three LLDs turn abruptly toward the alkali vertex at high F/M in the late stages of crystallization, but the calc-alkaline LLD has the flattest slope during the early stages of crystallization as a result of having the highest plagioclase/mafic mineral ratio (Fig. 7a) and the highest K_2O content. Nonetheless, even this rather extreme calc-alkaline composition does not produce a calc-alkaline trend. The LLD of the low-silica MORB′ composition is indistinguishable from that of the MORB composition until the latest stages of crystallization and is not shown. Thus initial silica content has minimal effect on the AFM trajectory of the LLD.

In order to illustrate the effects of magnetite crystallization, a simple empirical expression for the magnetite saturation surface (Appendix 1) was incorporated into the crystallization model and fractional crystallization of calc-alkaline composition was calculated with initial Fe^{3+} fractions of 0.1 and 0.2 FeO (total) by weight. The former yielded an initial f_{O_2} calculated with the algorithm of Kilinc et al. (1983) that was 0.2 log units below the quartz-fayalite-magnetite buffer; the latter Fe^{3+} content yielded an initial f_{O_2} 0.5 log units above the Ni-NiO buffer. The resulting LLDs are shown as dotted lines in Figure 7b. Both LLDs are kinked sharply toward the Alk vertex when magnetite (m) begins to crystallize. But in neither case does the bend toward the Alk vertex occur at low enough F/M to match the more extreme calc-alkaline trends (e.g., Carmichael et al., 1974). These results reinforce the conclusions of Grove et al. (1982) among others that simple closed system fractional crystallization of calc-alkaline liquids at low-pressure cannot produce calc-alkaline trends.

Figure 8 contains some of the more interesting oxide variation diagrams for the calculated LLDs. The mare LLD shows strong Fe enrichment coupled with silica depletion. The Fe enrichment is a reflection of the unbalanced shift of the ol-pl and lpyx-pl liquidus boundaries toward the Ol-Qtz join in Figure 7a as Mg′ decreases. This shift increases the proportion of the Fe-bearing components in the liquid. At low Mg′ the mafic components in the liquid are also low in SiO_2 (by weight), so SiO_2 concentration in the liquid decreases. Both the MORB and calc-alkaline LLDs show modest Fe and silica enrichments up to the point that ilmenite appears, at which point FeO concentration stabilizes and SiO_2 increases sharply. The calc-alkaline LLD shows the stronger silica increase and the weaker Fe enrichment—a reflection in part of the mild shift in ol-pl and lpyx-pl liquidus boundaries toward the Pl-Qtz join where the components are free of FeO and rich in SiO_2. Another factor affecting the variation of silica concentration is the proximity of the projected liquid composition to the Opx-Pl join (Fig. 7a) at the first appearance of low-Ca pyroxene: the farther to the high-Qtz side the liquid is, the more pronounced will be the subsequent silica enrichment. Accordingly, the short segment of calc-alkaline lpyx + aug + pl crystallization shows a much steeper rate of SiO_2 increase than the corresponding segment of the MORB LLD.

The MORB′ LLD shows Fe enrichment proportionately similar to the MORB LLD, but SiO_2 actually decreases during the crystallization of ol + pl + aug. This decrease is a reflection of the slow progress toward the Qtz{Wo} component evident in Figure 7a as well as the liquid becoming enriched in low-Mg′ components. Bulk compositions with lower initial silica and with similar Mg′, NOR, and NAB would show even stronger silica depletion, but would not crystallize low-Ca pyroxene unless magnetite precipitated soon after augite. Such compositions would either lie on the wrong side of the ol + pl + aug thermal divide or low-Ca pyroxene would be unstable in their low-Mg′ derivatives.

Na_2O and K_2O in Figure 8 show very different patterns. K_2O, which is excluded from all the crystallizing phases, more than doubles in all three LLDs, whereas Na_2O increases by less than a factor of 1.5. This weak increase is the result of Na_2O partition coefficients close to 1 for plagioclase-liquid pairs (Drake, 1976) in contrast to K_2O partition coefficients for calcic plagioclase that are typically in the range of 0.1 to 0.2 (e.g., Grove and Juster, 1989). Finally, despite the similarity of the MORB and mare trends in the TiO_2 vs. MgO plot, TiO_2 reaches a higher concentration along the mare LLD before the appearance of ilmenite, a reflection that the solubility of the ilmenite component is higher in more mafic liquids (Longhi, 1987a).

CRYSTALLIZATION DIAGRAMS

Many petrologists have become accustomed to inferring lines of descent from phase diagrams constructed from the projected compositions of multisaturated liquids produced in equilibrium experiments on crystallization and
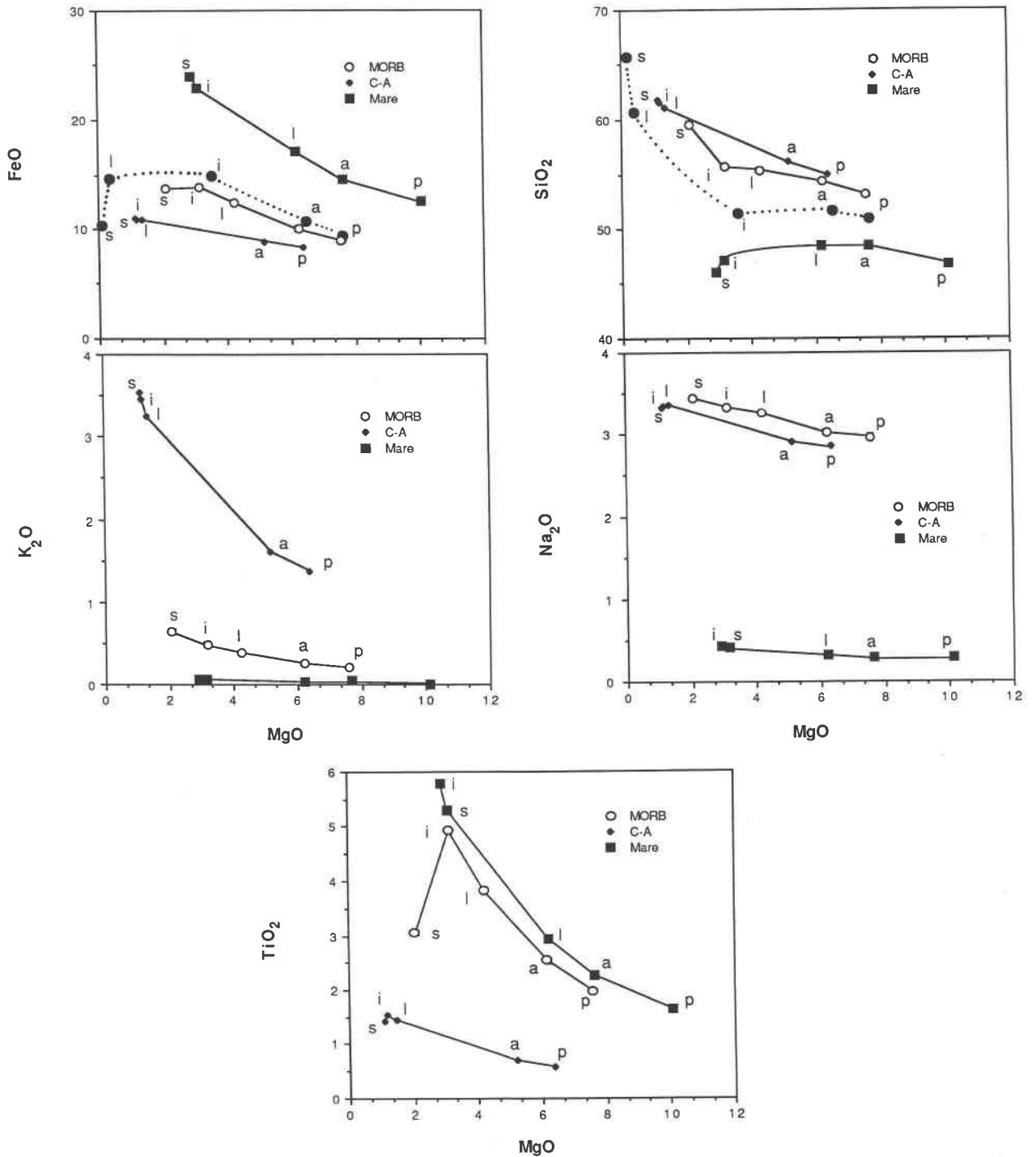
Fig. 8.   Oxide variation diagrams in weight percent. Small letters refer to appearance of new phases as in Figure 7. MORB' LLD is signified by solid circles and dotted lines.

melting. This is a simple and effective technique for the more primitive members of differentiation series because fractional and equilibrium crystallization paths will not have had the opportunity to diverge much. However, inferring the lines of descent of extensively fractionated liquids from equilibrium-path diagrams may lead to errors. In order to demonstrate the possibility of such errors,

calculations were performed for a calc-alkaline composition using an equilibrium crystallization program, and the liquid compositions at the first appearance of plagioclase, augite, low-Ca pyroxene, and silica were used to construct model liquidus diagrams. Figure 9 illustrates these diagrams in terms of {Wo} (Fig. 9a) and {Pl} (Fig. 9b) projections along with the calc-alkaline LLD from
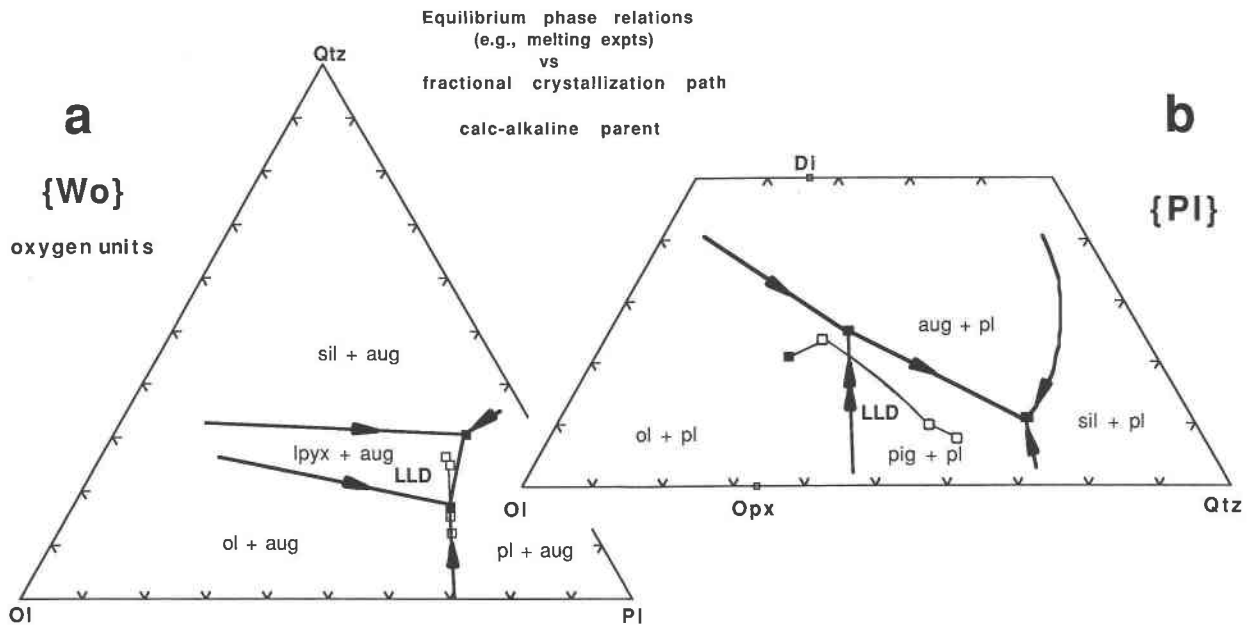
Fig. 9. Comparison of phase diagrams constructed from compositions of multisaturated liquids (filled squares) produced in equilibrium melting or crystallization experiments with calculated LLDs derived from same initial bulk composition (calc-alkaline parent). (a) LLD from Figure 7a. (b) LLD from Figure 6d.

Figures 6 and 7a, respectively. It is apparent that the LLD diverges from the equilibrium crystallization path toward lower Pl component in Figure 9a and toward lower Wo (or Di) component in Figure 9b. Silica also begins to crystallize at a much lower Qtz coordinate than would be predicted from the equilibrium path diagram. These differences between equilibrium and fractional crystallization paths are general features of magmatic differentiation.

There is also the possibility of confusing low- and high-pressure fractionation paths, if only the {Pl} projection is employed. Experiments on MORB (Stolper, 1980) and calc-alkaline compositions (Baker and Eggler, 1987) have shown that increasing pressure shifts the ol-pl-aug and lpyx-pl-aug boundaries to lower Wo contents, similar to the offset of the LLD from the liquidus boundaries in Figure 9b. However, these same studies show virtual independence of the positions of the same liquidus boundaries with increasing pressure up to 10 kbar when viewed in the {Wo} projection. Thus it may be difficult to distinguish a fractionation trend developed at low-pressure from one developed at crustal pressures under dry conditions, simply by comparing natural compositions to experimentally determined low-pressure liquidus boundaries. The situation is more favorable, however, for distinguishing trends developed under hydrous conditions because there is a definite shift of the ol-pl-aug and lpyx-pl-aug boundaries toward the Pl-Qtz join with increasing H_2O pressure (Baker and Eggler, 1987). In such cases it is possible to avoid potential errors in pressure estimates by employing both {Pl} and {Wo} projections together.

SUMMARY

Our knowledge of the topology of basaltic phase equilibria derived from studies of simple three- and four-component systems plus the extensive base of experimental data on natural compositions make accurate, empirical, quasi-linear parameterizations of basaltic liquidus boundaries possible. Parameterizing liquidus boundaries directly has an advantage over other approaches to predicting liquidus boundaries in that only surface equilibrium is assumed in the experimental data base, whereas thermodynamic (Ghiorso et al., 1983) and temperature-composition models (Nielsen, 1988) require equilibration of liquid and the portions of solid solutions that can be probed. Also, choosing projection coordinates as the major variables of the parameterizations greatly facilitates construction of phase diagrams, which in turn makes it possible to survey the systematic differences in phase equilibria among major groups of basalts, such as mare basalts, MORBs, and calc-alkaline basalts. These diagrams differ from familiar projections of liquidus boundaries based on experimental data in that important minor variables that have been shown to have the greatest effect on the positions of projected liquidus boundaries are held constant. These variables are Mg' and the alkali fractions of the normative feldspar, NAB and NOR. The diagrams generated by the parameterizations may thus be thought of as instantaneous representations of continuously evolving liquidus boundaries, whereas previously published liquidus diagrams are composites. The accurate range of the

parameterizations covers most of the range of hypersthene-normative basaltic compositions from Mg' = 0.7–0.1, NAB ≤ 0.6, NOR ≤ 0.5, and NAB + NOR ≤ 0.9. A major limitation of the model occurs at low Mg' and high values of NOR as the imminence of the two-liquid field induces curvatures in the various liquidus boundaries that the quasi-linear expressions cannot adequately represent. Graphic representation of two-liquid fields is also not possible with this approach, in which the minor variables are held constant, because liquid immiscibility strongly fractionates NAB and NOR.

When combined with empirical geothermometers for the phases of interest, the liquidus boundary parameterizations also lend themselves to rapid calculation of fractional and equilibrium crystallization (= partial melting in reverse). Comparison of calculations of fractional crystallization for mare, MORB, and calc-alkaline magmas with similar initial Mg' and crystallization sequence shows very different liquid lines of descent (LLD) with the mare LLD becoming more mafic and depleted in silica, whereas the calc-alkaline LLD becomes more felsic and enriched in silica; the MORB LLD maintains a nearly constant mafic/felsic ratio and shows modest silica enrichment. The LLDs also differ from their equilibrium crystallization paths, which petrologists commonly use to construct composite liquidus diagrams, in such a way as to mimic shifts in liquidus boundaries produced by elevated pressure. Thus there is the potential for confusing low- and high-pressure fractionations in anhydrous systems, if only composite phase diagrams are employed as discriminants.

References Cited

Baker, D.R., and Eggler, D.H. (1987) Compositions of anhydrous and hydrous melts coexisting with plagioclase, augite, and olivine or low-Ca pyroxene from 1 atm to 8 kbar: Application to the Aleutian volcanic center of Atka. American Mineralogist, 72, 12–28.

Bowen, N.L. (1915) The crystallization of haplobasaltic, haplodioritic, and related magmas. American Journal of Science, 40, 161–185.

Bowen, N.L., and Schairer, J.F. (1935) The system MgO-FeO-SiO$_2$. American Journal of Science, 229, 151–217.

Brady, J.B., and Stout, J.H. (1980) Normalizations of thermodynamic properties and some implications for graphical and analytical problems in petrology. American Journal of Science, 280, 173–189.

Carmichael, I.S.E., Turner, F.J., and Verhoogen, J. (1974) Igneous petrology, 739 p. McGraw-Hill, New York.

Drake, M.J. (1976) Plagioclase-melt equilibria. Geochimica et Cosmochimica Acta, 40, 457–465.

Emslie, R.F. (1971) Liquidus relations and subsolidus reactions in some plagioclase-bearing systems. Carnegie Institution of Washington Year Book, 69, 148–155.

Frost, B.R., Lindsley, D.H., and Andersen, D.J. (1988) Fe-Ti oxide–silicate equilibria: Assemblages with fayalitic olivine. American Mineralogist, 73, 727–740.

Ghiorso, M.S., Carmichael, I.S.E., Rivers, M.L., and Sack, R.O. (1983) The Gibbs free energy of mixing of natural silicate liquids; an expanded regular solution approximation for the calculation of magmatic intensive variables. Contributions to Mineralogy and Petrology, 84, 107–145.

Grove, T.L., and Bryan, W.B. (1983) Fractionation of pyroxene-phyric MORB at low pressure: An experimental study. Contributions to Mineralogy and Petrology, 84, 293–309.

Grove, T.L., and Juster, R. (1989) Experimental investigation of low-Ca pyroxene stability and olivine-plagioclase-liquid equilibrium at 1-atm in natural basaltic and andesitic liquids. Contributions to Mineralogy and Petrology, 103, 287–305.

Grove, T.L., Gerlach, D.C., and Sando, T.W. (1982) Origin of calc-alkaline series lavas at Medicine Lake volcano by fractionation, assimilation and mixing. Contributions to Mineralogy and Petrology, 80, 160–182.

Hess, P.C., Rutherford, M.J., Guillemette, R.N., Ryerson, F.J., and Tuchfeld, H.A. (1975) Residual products of fractional crystallization of lunar magmas: An experimental study. Proceedings of the Sixth Lunar Science Conference, 895–910.

Hess, P.C., Rutherford, M.J., and Campbell, H.W. (1978) Ilmenite crystallization in non-mare basalt: Genesis of KREEP and high-Ti basalt. Proceedings of the Ninth Lunar and Planetary Science Conference, 705–724.

Irvine, T.N. (1970) Crystallization sequences in the Muskox intrusion and other layered intrusions, I. Olivine-pyroxene-plagioclase relations. Geological Society of South Africa, Special Publication 1, 441–476.

—— (1976) Metastable liquid immiscibility and MgO-FeO-SiO$_2$ fractionation patterns in the system Mg$_2$SiO$_4$-Fe$_2$SiO$_4$-CaAl$_2$Si$_2$O$_8$-KAlSi$_3$O$_8$-SiO$_2$. Carnegie Institution of Washington Year Book, 75, 597–611.

—— (1980) Magmatic density currents and cumulus processes. American Journal of Science, 280A, 1–58.

Jackson, E.D. (1961) Primary textures and mineral associations in the ultramafic zone of the Stillwater Complex, Montana. United States Geological Survey Professional Paper 358, 106 p.

Kilinc, A., Carmichael, I.S.E., Rivers, M.L., and Sack, R.O. (1983) The ferrous-ferric ratio of natural silicate liquids equilibrated in air. Contributions to Mineralogy and Petrology, 83, 136–140.

Langmuir, C.H., and Hanson, G.N. (1981) Calculating mineral-melt equilibria with stoichiometry, mass balance and single component distribution coefficients. In R.C. Newton, A. Navrotsky, B.J. Woods, Eds., Thermodynamics of minerals and melts, p. 247–272. Springer-Verlag, New York.

Longhi, J. (1977) Magma oceanography 2: Chemical evolution (abs.). Lunar Science VIII, 592–594.

—— (1982) Effects of fractional crystallization and cumulus processes on mineral composition trends of some lunar and terrestrial rock series. Journal of Geophysical Research, 87, A54–A64.

—— (1987a) On the connection between mare basalts and picritic volcanic glasses. Journal of Geophysical Research, 92, E349–E360.

—— (1987b) Liquidus equilibria and solid solution in the system Anorthite-Forsterite-Wollastonite-Silica at low pressure. American Journal of Science, 287, 265–331.

—— (1990) Silicate liquid immiscibility in isothermal crystallization experiments. Proceedings of the 20th Lunar Planetary Science Conference, 7–24.

Longhi, J., and Pan, V. (1988a) A reconnaissance study of phase boundaries in low-alkali basaltic liquids. Journal of Petrology, 29, 115–148.

—— (1988b) Phase equilibrium constraints on the howardite-eucrite-diogenite association. Proceedings of the 18th Lunar Planetary Science Conference, 459–470.

—— (1989) The parent magmas of the SNC meteorites. Proceedings of the 19th Lunar Planetary Science Conference, 451–464.

Longhi, J., Walker, D., and Hays, J.F. (1978) Fe and Mg distribution between olivine and lunar basaltic liquids. Geochimica et Cosmochimica Acta, 42, 1545–1558.

Morse, S.A. (1980) Basalts and phase diagrams, 493 p. Springer-Verlag, New York.

Nielsen, R.L. (1988) A model for the simulation of combined major and trace element liquid lines of descent. Geochimica et Cosmochimica Acta, 52, 27–38.

Nielsen, R.L., and Dungan, M.A. (1983) Low pressure mineral-melt equilibria in natural anhydrous mafic systems. Contributions to Mineralogy and Petrology, 84, 310–326.

O'Hara, M.J. (1968) The bearing of phase equilibria studies in synthetic and natural systems on the origin and evolution of basic and ultrabasic rocks. Earth Science Reviews, 4, 69–133.

Presnall, D.C., Dixon, S.A., Dixon, J.A., O'Donnell, T.H., Brenner, N.L., Schrock, R.L., and Dycus, D.W. (1978) Liquidus relations on the join diopside-forsterite-anorthite from 1 atm to 20 kbar: Their bearing on the generation of and crystallization of basaltic magma. Contributions to Mineralogy and Petrology, 66, 203–220.

Raedeke, L.D., and McCallum, I.S. (1984) Investigations of the Stillwater Complex. Part II. Petrology and petrogenesis of the ultramafic zone. Journal of Petrology, 25, 395–420.

Roeder, P.L. (1975) Thermodynamics of element distribution in experimental mafic silicate-liquid systems. Fortschrifte für Mineralogie, 52, 61–73.

Roeder, P.L., and Emslie, R.F. (1970) Olivine-liquid equilibrium. Contributions to Mineralogy and Petrology, 29, 275–289.

Stolper, E.M. (1977) Experimental petrology of eucritic meteorites. Geochimica et Cosmochimica Acta, 41, 587–611.

——— (1980) A phase diagram for mid-ocean ridge basalts: Preliminary results and implications for petrogenesis. Contributions to Mineralogy and Petrology, 74, 13–27.

Walker, D., Longhi, J., and Hays, J.F. (1972) Experimental petrology and origin of Fra Mauro rocks and soil. Proceedings of the Third Lunar and Science Conference, 797–817.

Walker, D., Shibata, T., and DeLong, S.E. (1979) Abyssal tholeiites from the Oceanographer Fracture Zone II: Phase equilibria and mixing. Contributions to Mineralogy and Petrology, 70, 111–125.

APPENDIX 1.

The empirical expressions employed in this paper are modifications of expressions presented previously by Longhi (1987a) and Longhi and Pan (1988b). The basis for the set of equations for silicate minerals is the set of liquidus boundaries in the pseudoquaternary system Ol-Pl-Wo-Qtz. This system involves a projection from (i.e., ignoring) TiO_2, Cr_2O_3, the orthoclase component (Or), and other minor constituents. The system coordinates chosen to be the major variables are the quaternary wollastonite component (Wo) and the olivine and quartz coordinates projected from the Wo component, Ol{Wo} and Qtz{Wo}. Equations for these variables in mole units are as follows:

$$Wo = \frac{(CaO - Al_2O_3 + K_2O + Na_2O)}{(SiO_2 - Al_2O_3 - 5K_2O - 3Na_2O)}$$
$$\Sigma = SiO_2 - CaO - 6K_2O - 4Na_2O$$
$$Ol\{Wo\} = 0.5(FeO + MgO + MnO + 2Fe_2O_3)/\Sigma$$
$$Qtz\{Wo\} = [SiO_2 - 0.5(FeO + MgO + MnO + 2Fe_2O_3)$$
$$- Al_2O_3 - CaO - 5(K_2O + Na_2O)]/\Sigma$$
$$Pl\{Wo\} = 1 - Ol\{Wo\} - Qtz\{Wo\}.$$

The minor variables are the normalized Fe-Mg ratio

$$Fe' = FeO/(FeO + MgO)$$

the albite fraction in the normative feldspar

$$NAB = 2Na_2O/(Al_2O_3 + Na_2O + K_2O)$$

and the orthoclase fraction in the normative feldspar

$$NOR = 2K_2O/(Al_2O_3 + Na_2O + K_2O).$$

Although the phase boundary parameterizations are in terms of mole units, O units employed in the figures because O units reproduce volume proportions of minerals and because mole units may appear to vary nonlinearly in projection (Brady and Stout, 1980; Longhi and Pan (1988a). To convert mole units to O units, simply multiply each molar coordinate by the number of O atoms in its formula and renormalize.

The various new parameterizations of liquidus boundaries in mole units are as follows:

olivine-plagioclase: $Ol\{Wo\} = a \cdot Qtz\{Wo\} + b \cdot Wo + c$

$a = -0.528[1 - 0.6NAB - 20.2NAB \cdot NOR^3 + 27NAB$
$\quad \cdot NOR^5 - 3NOR^2(NOR - NAB)^2$
$\quad + 10NOR^2(NAB - NOR)^3] \cdot (1 + 0.54Fe')$

$b = 0.10(1 - 1.67Fe')$

$c = 0.50 + 0.29Fe' + 0.013Fe'^4 - (1 + 0.18Fe')$
$\quad \cdot [0.31NAB + NAB(0.45NOR + NOR^2 + 19NOR^4$
$\quad - 11NOR^5 - 40NOR^7) + 2NOR^2$
$\quad \cdot (NOR - NAB)^2 + 3NOR^2(NOR - NAB)^3]$

olivine-low-Ca pyroxene: $Qtz\{Wo\} = a \cdot Ol\{Wo\} + b \cdot Wo + c$, where

$a = [0.8 - 3Fe'^2 + 2Fe'^4 - 2NOR^2(1 - NAB)^2]/$
$\quad [1 + 2NOR^2(1 - NAB)^2]$

$b = 0.25(1 - 1.67Fe')/[1 + 2NOR^2(1 - NAB)^2]$

$c = [0.188 + 0.534Fe'^2 + 0.844Fe'^4 - 1.12Fe'^6 - 0.4NOR$
$\quad \cdot NAB^2 + 2NOR^2(1 - NAB)^2]/[1 + 2NOR^2(1 - NAB)^2]$

low-Ca pyroxene-plagioclase: $Ol\{Wo\} = a \cdot Qtz\{Wo\} + b \cdot Wo + c$

$a = -0.68(1 + 0.45Fe')$
$\quad \cdot [1 - 0.6NAB - 23.6NAB \cdot NOR^3 + 50NAB \cdot NOR^5$
$\quad - 10NOR^2(NOR - NAB)^2 - 5NOR^2(NOR - NAB)^3]$

$b = 0.1(1 - 1.67Fe')$

$c = 0.57 + 0.29Fe' + 0.04Fe'^4 - (1 + 0.18Fe')$
$\quad \cdot [3NOR^2(NOR - NAB)^2 + 4NOR^2(NOR - NAB)^3$
$\quad + 0.315NAB + NAB$
$\quad \cdot (0.71NOR + NOR^2 + 29NOR^4 - 57NOR^5 +$
$\quad 55NOR^7)]$

olivine-augite: $Wo = d \cdot Ol\{Wo\} + e \cdot Qtz\{Wo\} + f + k(1 - Pl\{Wo\})^n$, where

$d = 0.54(1 - 0.05NAB)$

$e = -0.158(1 - 0.8Fe' - 0.8NAB + 0.2NOR \cdot NAB)$

$f = 0.16 - 0.2Fe' + 2NAB$
$\quad \cdot (0.11NOR - NOR^2 + 0.8NOR^3 + 0.7NOR^4)$
$\quad - 4.9NOR^2(NOR - NAB)^2 - 0.6(NAB - NOR)$
$\quad \cdot (1 - NAB - NOR)^2$

$k = 0.1 \quad n = 6$

low-Ca pyroxene-augite: $Wo = d \cdot Ol\{Wo\} + e \cdot Qtz\{Wo\} + f + k(1 - Pl\{Wo\})^n$, where

$d = 0.45(1 - 0.05NAB + 0.3NAB \cdot NOR + 0.05Fe')$

$e = 0.22[1 + 0.2Fe' + 2NAB(- 5.4NOR^2 + 2.9NOR^4)$
$\quad - 0.75NAB - 2NOR^2(NOR - NAB)^2$
$\quad - 8NOR^2(NOR - NAB)^3]$

$f = 0.06 - 0.2Fe' + 0.34NAB^2 - 0.67NAB^4$
$\quad + 2NAB(0.12NOR - 0.85NOR^2 + 3.9NOR^3)$

$$- 0.6(NOR - NAB)\cdot(1 - NOR - NAB)^2$$
$$- 4NOR^2(NOR - NAB)^2 - 6NOR^2(NOR - NAB)^3$$
$$k = 0.1 \quad n = 6$$

orthopyroxene-pigeonite: $Wo = a\cdot Ol\{Wo\} + b\cdot Qtz\{Wo\} + c$

$$a = 0.1 - 0.5NAB \qquad b = -0.175(1 - NAB)$$
$$c = 0.297 + 0.1Fe' - 0.85(1 - 2.1NOR^2)\cdot Fe'^2$$
$$- 0.02(NAB)^{1/2} + 0.3NAB^2$$

silica-low-Ca pyroxene: $Qtz\{Wo\} = a\cdot Ol\{Wo\} + b\cdot Wo + c$, where

$$a = [-0.3 + 0.14Fe' + 0.08Fe'^2 - 0.4(NAB + NOR)]/$$
$$[1 + 0.4(NAB + NOR)]$$
$$b = 0.333(1 - 1.14Fe')/[1 + 0.4(NAB + NOR)]$$
$$c = [1.084 - 0.159Fe' + 0.0542Fe'^2 + 0.0256Fe'^3$$
$$+ 0.4(NAB + NOR) - 0.9(NAB + NOR)\cdot Fe'^2$$
$$+ 10NOR^2\cdot(1 - Fe')\cdot(NOR - NAB)^2]$$
$$\cdot[1 + 0.4(NAB + NOR)].$$

For high-Ti liquids ($TiO_2 > 4$ mol%), the following expressions apply:

olivine-low-Ca pyroxene:	$Qtz\{Wo\}$ (high-Ti) = $Qtz\{Wo\}$ (low-Ti) $- 0.0125(TiO_2 - 4.0)$
olivine-plagioclase:	$Ol\{Wo\}$ (high-Ti) = $Ol\{Wo\}$ (low-Ti) $+ 0.009(TiO_2 - 4.0)$
olivine-augite:	Wo (high-Ti) = Wo (low-Ti) $- 0.0125(TiO_2 - 4.0)$
low-Ca pyroxene-plagioclase:	$Ol\{Wo\}$ (high-Ti) = $Ol\{Wo\}$ (low-Ti) $+ 0.009(TiO_2 - 4.0)$
low-Ca pyroxene-augite:	Wo (high-Ti) = Wo (low-Ti) $- 0.0125(TiO_2 - 4.0)$.

Convenience of manipulation of the expressions in the crystallization programs determines which system variable is treated as the independent variable in these equations. These equations have been developed over the years largely through trial and error. In general, the exponential terms are insignificant when the relevant minor variable is close to 0; the higher order terms dampen or even reverse the rate of increase of the lower order terms as the minor variables approach 1.0. The initial sets of expressions were derived to model primitive lunar magmas with low NAB and NOR (e.g., Longhi, 1977, 1982) and the only minor variable was Fe'. Subsequent versions introduced TiO_2 (Longhi, 1987a) to account for high-Ti mare basalts, NAB and NOR combined as a single variable (Longhi and Pan, 1988b) to account for MORB-like compositions, and NAB and NOR as separate variables (Longhi and Pan, 1989) to account for both MORB and calc-alkaline compositions. The 1989 version was generally adequate for terrestrial basalts, where NAB > NOR, but not, however, for the case of low NAB and NAB < NOR, which is encountered in evolved KREEP magmas. This shortcoming necessitated the addition of one or two terms of the form

$$aNOR^2(NOR - NAB)^2 + bNOR^2(NOR - NAB)^3$$

which is insignificant when NOR is low and tend to cancel when NAB > NOR, but become significant when NAB < NOR.

The expression for the ilmenite-saturation surface employed in this paper is modified slightly from the version derived previously by Longhi (1987b) and is derived by sequential multiregression on both lunar and terrestrial compositions. The variables in this formulation are based upon a projection from the Pl component into the Pyx-Ilm-FmO system. Projection coordinates are

$$\Sigma = FeO + MgO + MnO + 2Fe_2O_3 + CaO$$
$$- Al_2O_3 + Na_2O + K_2O$$
$$FmO\{Pl\} = [FeO + MgO + MnO + 2Fe_2O_3 + CaO$$
$$+ Al_2O_3 + 5(Na_2O + K_2O) - SiO_2 - TiO_2]/\Sigma$$
$$Ilm\{Pl\} = TiO_2/\Sigma.$$

The expression for the ilmenite surface based on 41 points is

$$Ilm\{Pl\} = -0.450Fe' - 0.197ALK - 0.0215FmO\{Pl\}$$
$$+ 0.515 \qquad R^2 = 0.931$$

where ALK is alkali feldspar fraction of the system

$$ALK = 2(Na_2O + K_2O)/[FeO + MgO + MnO + 2Fe_2O_3$$
$$+ CaO + 5(Na_2O + K_2O)].$$

A preliminary expression for the magnetite-saturation surface at the QFM buffer has been derived from the data of Grove et al. (1982), Baker and Eggler (1987), and Grove and Juster (1989). This expression is cast in terms of an eight-component system: Qtz-FmO-Ab-Or-An-Wo-TiO$_2$-Mgt. The requisite coordinates are

$$\Sigma = SiO_2 + TiO_2 - Al_2O_3 + FeO + MgO$$
$$+ MnO - 3(Na_2O + K_2O)$$
$$FmO = (FeO + MgO + MnO - Fe_2O_3)/\Sigma$$
$$Qtz = [SiO_2 - Al_2O_3 - CaO - 5(Na_2O + K_2O)]/\Sigma$$
$$Mgt = Fe_2O_3/\Sigma.$$

The expression for the magnetite surface based on 12 points is

$$Mgt = 0.150FmO - 0.0347Fe^* - 0.0536 + 0.0401$$
$$R^2 = 0.927$$

where

$$Fe^* = (FeO + 2Fe_2O_3)/(FeO + MgO + 2Fe_2O_3).$$

Appendix Figure 1 illustrates the success with which the various expressions predict the graphical positions of multisaturated liquids given only the composition of the liquids taken from the literature. Liquids saturated with three or four phases appear in more than one diagram, e.g., a liquid saturated with ol, plag, and aug will appear in the ol/plag and ol/aug diagrams. Because of the paucity of data on liquids saturated with both orthopyroxene and pigeonite, the pi/opx diagram illustrates bracketing of the boundary: opx-saturated liquids should plot with Wo coordinates ≥ 0, whereas pig-saturated liquids should plot with Wo coordinates ≤ 0. In an analogous fashion, the data of Baker and Eggler (1987) bracket the ol-lpyx boundary in the ol-lpyx diagram: the small open squares are liquids saturated with olivine; the squares with crosses are liquids saturated with orthopyroxene. Error bars permit an evaluation of the effects of several analytical and experimental errors as well as approximate conversion of graphical coordinates into weight percents of the most critical oxides.

Not surprisingly, the most accurate expressions appear to be those for ol-pl and ol-aug. Commonly encountered errors, such as loss of Fe to Pt loops, volatilization of alkalies, and routine variations in the measurement of SiO_2, have relatively minor effects on the positions of these phase boundaries. The lower viscosities of olivine-saturated liquids also facilitate more rapid equilibration and the growth of fewer, but larger crystals, which makes for more reliable microprobe analyses. The largest uncertainties are encountered in predicting the ol-lpyx boundary, in large part because the compositional vectors produced by major experimental errors are nearly normal to the ol-lpyx boundary, e.g., the Fe-loss vector is parallel to the Ol-Qtz join in the {Wo}
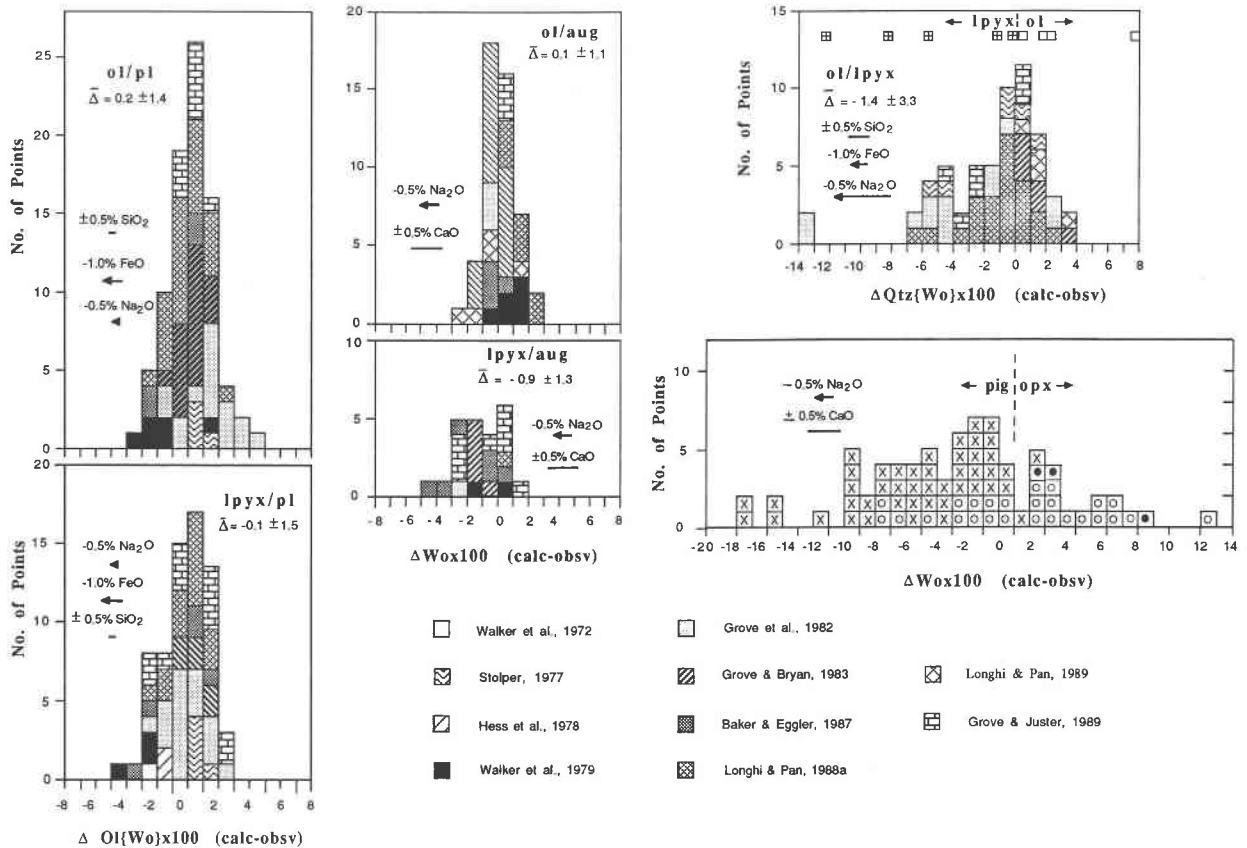
Appendix Fig. 1. Comparison of calculated and reported values of the various liquidus phase boundaries in terms of relevant projection coordinates. Wo is the quaternary wollastonite component in the Ol-Pl-Wo-Qtz model system (Fig. 2). Ol{Wo} and Qtz{Wo} are coordinates of the Ol-Pl-Qtz ternary projected from the Wo component. Bars indicate the magnitude of the indicated weight percent errors; arrows indicate unidirectional errors, such as Fe and alkali loss. With the exception of the pig/opx diagram and the smaller squares at the top of the lpyx/ol figure, all of the boxes represent liquids saturated with at least the two phases indicated in the figure. The two exceptions are for bracketing experiments in which only one of the two phases is present. In the lpyx/ol diagram open squares signify olivine, whereas squares with crosses signify orthopyroxene. In the pig/opx diagram, X = pigeonite only, O = orthopyroxene only (data from references in Figs. 5 and 6), and filled O = opx + pig (Grove and Juster, 1989).

projection and the Na_2O and SiO_2 vectors are radial to the Qtz apex. The unidirectional nature of the Fe-loss and Na_2O volatilization errors is also consistent with the skewed distribution of errors toward negative values of $\Delta Qtz\{Wo\}$ in the ol-lpyx diagram. In addition, some of the spread in the data appears to be attributable to systematic interlaboratory differences in microprobe analyses, as suggested in the ol-pl diagram where there is a systematic offset between the data of Walker et al. (1979) and those of Grove and Bryan (1983) even though the experimental techniques and compositions investigated (MORB) were similar. Finally, some of the deviations in these histograms are undoubtedly the result of the basically linear nature of the empirical equations. We know from studies of simple systems that some liquidus boundaries are strongly curved and attempting to fit this curvature with linear equations will inevitably lead to errors. Predictably, the most pronounced curvatures are likely to occur in the vicinity of stable or metastable two-liquid fields (Irvine, 1976) and affect liquids at or near silica saturation with high Fe'. Such liquids are likely to be the products of extreme fractional crystallization and thus not in the provenance of a basaltic model in the strict sense; however, any extensions of the model to these residual compositions will require nonlinear terms in the phase boundary expressions.

In order to model crystallization processes, it is necessary to combine the phase boundary parameterizations described above with various empirical algorithms to calculate liquidus temperature and phase compositions. Some of these are as follows: olivine composition is calculated from the empirical expressions of Longhi et al. (1978); plagioclase is calculated from the expressions of Drake (1976) plus an assumed molar partition coefficient for K_2O of 0.1; pyroxenes are calculated from the partition coefficient regressions of Longhi and Pan (1989); oxides are calculated from the partition coefficients summarized by Longhi (1987a); liquidus temperatures of olivine-saturated liquids are calculated by first determining the olivine composition independent of temperature and then solving for temperature using the temperature-composition equation for olivine + liquid (Longhi et al., 1978); temperatures of olivine-free, lpyx-saturated liquids are calculated from a simple empirical relationship based on the data of Walker et al. (1979). Each crystallization step consists of equilibrium crystallization of 1 mol% of the remaining liquid, followed by removal of the crystals (fractional crystallization) or addition of the crystals to those previously crystallized (equilibrium crystallization); proportions of saturating phases are varied in successive steps to maintain liquid compositions close to the phase boundaries.